Cell Biology International

WILEY

Cell Biology International

RESEARCH ARTICLE

Mammary Gland Reactive Stroma Characterization at Aging After Bisphenol A Exposure During Hormonal Susceptibility Windows

Gervásio Evangelista Brito Filho[1] | Thalles Fernando Rocha Ruiz[1,2] | Lorena Gabriela de Souza[1] | Luara Jesus Ferrato[1] | Fernanda Cristina Alcantara dos Santos[3] | Patricia Simone Leite Vilamaior[1] | Ellen Cristina Rivas Leonel[3,4] | Sebastião Roberto Taboga[1,2]

[1]Microscopy and Microanalysis Center, Institute of Biosciences, Letters and Exact Sciences (IBILCE), São Paulo State University (Unesp), São José do Rio Preto, SP, Brazil | [2]Institute of Biosciences (IB), University of Campinas (UNICAMP), Campinas, SP, Brazil | [3]Department of Histology, Embryology and Cell Biology, Institute of Biological Sciences (ICB III), Federal University of Goiás – UFG, Goiânia, GO, Brazil | [4]Animal Molecular and Cellular Biology, Louvain Institute of Biomolecular Science and Technology, Université catholique de Louvain, Louvain-la-Neuve, Belgium

Correspondence: Thalles Fernando Rocha Ruiz (thalles.ruiz@unesp.br) | Sebastião Roberto Taboga (sebastiao.taboga@unesp.br)

Received: 15 October 2024 | **Revised:** 30 December 2024 | **Accepted:** 13 January 2025

Funding: Fundação de Amparo à Pesquisa do Estado de São Paulo – Brazil (FAPESP), Grant Numbers: 2023/16098-1 (GEFB), 2022-00521-0 (TFRR), 2021/14140-5 (SRT); National Council for Scientific and Technological Development – Brazil (CNPq): Institutional Scientific Initiation Scholarship Program (PIBIC), Grant Number PROPe 04/2022; and Grant Number 302938/2020-6 (SRT).

Keywords: aging | BPA | endocrine disruptor | fibroblasts | telocytes

ABSTRACT

Mammary glands development is influenced by endocrine signaling, which remodels epithelial and stromal compartments. Reactive stroma phenotype is observed when stromal disturbances occur, leading to changes in extracellular matrix composition and occurrence of reactive cell types. One of the triggers of these alterations is endocrine-disrupting chemical exposure, such as bisphenol A (BPA). Studies suggest that BPA acts on receptor binding sites of several hormones interfering the endocrine response. The aim of this study was to investigate the reactive stroma features on mammary glands of aged female gerbils (*Meriones unguiculatus*) exposed to BPA during windows of susceptibility. Thus, the analysis of cellular profile and growth factor expressions was provided. Fibroblastic population changed in BPA-exposed mammary glands, with a remarkable increase of myofibroblasts (vimentin$^+$/α-SMA$^+$) and active fibroblasts (FAP$^+$). Normal fibroblasts (vimentin$^+$/α-SMA$^-$) were decreased mainly associated with the increase of FGF-10, an inductor of fibroblastic polarization. CD34$^+$ stromal cells were also identified and detected among epithelial cells after BPA-induction disruption. Angiogenesis was supported by VEGF increasing in the gland tissue, which promoted an increase in blood vessel density. Thus, our results demonstrated that reactive stroma was raised in the mammary gland after BPA exposure. This profile was supported by changes in the fibroblastic population due to an induction to synthetic phenotypes and the expression of FGF-10, as well as the angiogenic activity that could corroborate with the malignancy and aggressiveness induced by BPA exposure.

1 | Introduction

Mammary glands are tubule alveolar apocrine glands, mainly constituted of glandular epithelial tissue (20%–30%) involved by myoepithelial and basal cells (Macias and Hinck 2012; Vandenberg 2021), and surrounded by a connective tissue, known as stroma (Biswas et al. 2022). The gland development and activity are hormone-dependent (Musumeci et al. 2015),

Gervásio Evangelista Brito Filho and Thalles Fernando Rocha Ruiz contributed equally to this study.

which remodel tissue compartments in alternated phases for growth, differentiation, and involution. The major components remodeling relates to the connective tissue, since it is responsible not only for support but also for the paracrine signaling for epithelial development, modulation, and functional targeting (Godfrey 2009). Its composition varies according to the tissue, presenting structural, cellular, and noncellular components quantity differences (Theocharis et al. 2016). The noncellular components, as collagen and elastic fibers, are secreted by fibroblasts population. The mammary gland stroma thereby regulates proliferation, development, and differentiation in this gland, through synthesis and/or activation of some collagen types, hormones, and growth factors secretion and by expression of matrix metalloproteinases (Xu, Boudreau, and Bissell 2009). Thus, stroma acts both as an epithelial physical support and a tissue functional and morphological driver, also maintaining the organ homeostasis (Tuxhorn et al. 2001; Vandenberg 2021).

Several adverse conditions, such as exposition to endocrine-disrupting chemicals that promote disturbances in the mammary gland, triggers important epithelial, and stromal changes. When neoplastic development occurs, stroma homeostasis is affected, leading to hypervascularization and changes in extracellular matrix components, condition known as reactive stroma (Barron and Rowley 2012; Bussard et al. 2016). The reactive stroma is characterized by the occurrence and/or differentiation of novel cellular types, alteration, and increase in healthy tissue present cellular types (e.g., increase and changes in fibroblasts smooth muscle cells and mesenchymal stem cells), promoting signals to tumoral development and growth and neoplastic cells invasion (Brivio et al. 2017; San Martin et al. 2014).

In the reactive stroma, two main cell types are commonly observed. First, the activated fibroblasts, which present intense expression of fibroblast activation protein (FAP), promoting a high rate of extracellular matrix elements secretion (Kalluri and Zeisberg 2006). Also, the cancer associated fibroblasts (CAFs), which have a continuous activation character and extracellular matrix cytokines and components secretion (Brivio et al. 2017). This cell presents a high expression of cell markers, such as vimentin, smooth muscle α-actin (α-SMA), FAP, and fibroblast growth factor 10 (FGF-10) (Cui and Li 2013; Nissen, Karsdal, and Willumsen 2019).

One of the most studied endocrine-disrupting chemical molecules is bisphenol A (BPA). BPA is one of the best known and worldwide distributed endocrine-disrupting chemicals, with major production intensity (Abraham and Chakraborty 2019). BPA is a petroleum-derived molecule present especially in polycarbonate plastics and epoxy resins (Bujalance-Reyes et al. 2022; Huang et al. 2012), which can also be used as an additive to other plastic types (Staples et al. 1998). Due to its wide employment, BPA can be identified in different sources, such as water and food, owing to anthropogenic only processes, being observed at high rates in industrial and densely populated areas (Abraham and Chakraborty 2019; Lalonde and Garron 2020).

Some studies demonstrated that BPA exposition presents effects mainly connected to reproductive parameters (Manfo et al. 2014; Oehlmann et al. 2009). Its exposition was also associated to cardiovascular diseases, diabetes (Huang et al. 2012), insulin resistance, and low glycose tolerance (Bujalance-Reyes et al. 2022; Lind and Lind 2018). Mammary gland and prostate pre-neoplastic alterations were also linked to this compound, besides acting as a strong estrogen-like agent (Leonel et al. 2020; Vandenberg et al. 2007). BPA has known effects for changing involution time, altering the stromal compartment, extracellular matrix components, and worsening inflammation (Ruiz et al. 2022). Also, it causes disturbances in hormonal reception and signaling of estrogen and androgen, as well as changing epigenetic response (Ruiz, Taboga, and Leonel 2021). Previous studies of our research group indicated that exposure to BPA during pregnancy and lactation promotes the development of malignant features in the mammary gland at aging, with a remarkable remodeling on the extracellular matrix fibers network (Ruiz et al. 2021). Thus, the present study aimed to evaluate reactive stroma cell types and growth factors related to tissue remodeling, morphological changes, and angiogenesis in aged female Mongolian gerbil exposed to BPA during windows of susceptibility.

2 | Materials and Methods

2.1 | Experimental Model and Sample Processing

In the present study, Mongolian gerbil females ($N = 15$) were kept in BPA-free polysulfone cages, according to the manufacturer's specifications (Alesco), during all experimental periods. Those cages were placed on ventilated shelves, under a 12 h light/shadow period and controlled temperature. Animals were provided with *ad libitum* water and food. Females were allocated with fertile males and submitted to daily gavage for 39 days period, corresponding to gestational period (24–26 days) and lactation (21 days). To establish the onset of pregnancy, females had their 1st litter discarded and after 8 days, when occurs the blastocyst implantation (Norris and Adams 1972), the treatment was started. Then, the animals were subdivided into thre groups: Control ($n = 5$): 0.1 mL water gavage; Vehicle ($n = 5$): 0.1 mL corn oil gavage; BPA ($n = 5$): gavage of BPA diluted in corn oil (50 μg/kg). The BPA dosage—50 μg/kg/day—was considered as a pro-carcinogenic dose for mammary glands (Ruiz, Taboga, and Leonel 2021; Ruiz, Taboga, and Leonel 2021; Ruiz et al. 2022; Ruiz, Taboga, and Leonel 2021; Ruiz et al. 2023), considered a safe dose according to the United States Environmental Protection Agency (USEPA; Hu et al. 2022) in the study realization period. This dose was reduced to 2 ng/kg/day, which is currently the safe dose according to the European Food Safety Authority (EFSA; EFSA Panel on Food Contact Materials, Enzymes and Processing Aids et al. 2023). At 18 months, in aged period of life, all females were weighed, anesthetized with 3% isoflurane in O_2 and euthanized by decapitation.

Mammary glands were then collected and fixed in paraformaldehyde 4% for 24 h and processed under standard histology procedures or fixed in glutaraldehyde 2.5% for electron microscopy technique. This study followed Ethic Committee in Animal Utilization (CEUA) procedures, under the protocol n° 217/2019.

2.2 | Cytochemistry Analysis

For the histological analysis, the samples fixed in paraformaldehyde 4% were destined to tissue paraffin inclusion realized in Leica Automatic System (TP 1020), and paraffin blocks were prepared in the Leica Inclusion Central (1150 H). The blocks were sectioned using a Leica automatic rotating microtome (RM 2255) at 5 μm thin, lied on silanized slides for histology and immunohistochemistry analysis.

To evaluate stromal vascularization, Gomori trichrome stain was performed due to the strong red blood cells staining (red) and a blue staining to collagen fibers (blue). To this stain technique, slides used were submitted to standard histology protocol to deparaffinization and rehydration, then in blue Gomori stain, washed in distilled water, counterstained with hematoxylin, washed, dehydrated, and mounted with Canada balsam. To quantify the blood vessels' frequency, the M130 multipoint test (WEIBEL 1963) was employed to evaluate tissue vascularization (a total of 10 photos of each sample were randomly taken, totalizing 50 photos per group and 150 total fields per group at 400x magnification).

2.3 | Immunohistochemistry

This technique was employed to evaluate the expression of growth factors, vascular endothelial growth factor (VEGF) and FGF-10, as well as for the identification of cell clusters FAP^+ (activated fibroblasts) and $CD34^+$ stromal cells. The following protocol was followed, with PBS (VEGF, CD34; with tween addition; pH = 7.4) or TBS (FGF-10, FAP; pH = 7) buffer washes between each step: sample rehydration by submerging the slides in xylene, xylene/alcohol, a decreased progression of alcohols, and water for rehydration. Then, citrate buffer (10 mM) was added to the slides and submerged in a heated water bath (92°C–98°C) for antigen recovery. For peroxidase blocking, 10% H_2O_2 in methanol was used. Nonspecific proteins were blocked using a solution of 5% skimmed milk in the wash buffer. Then, the primary antibodies were diluted with BSA 1% (in PBS/TBS) and left overnight: VEGF (1:50, sc-152, rabbit polyclonal, Santa Cruz Biotechnology Inc., United States); FGF-10 (1:50, sc-7375, Santa Cruz Biotechnology Inc., United States, goat polyclonal); FAP (1:50, sc-65398, Santa Cruz Biotechnology Inc., United States, mouse monoclonal); CD34 (1:50, Invitrogen, PA5-85917, VH3062113, rabbit polyclonal). After that, the secondary antibody was added to the samples to incubation and polymer link (polymer detection system Novolink™, Leica Biosystems Newcastle Ltd., Newcastle, United Kingdom). Antigen-protein binding was observed by reaction with DAB (1:100, 3′-3′diaminobenzidine; Novolink™ DAB, RE7270-CE, Leica Biosystems, Buffalo 121 Grove, United States) and counterstained with hematoxylin. To quantify the VEGF, as well as FAP^+ and $CD34^+$ cells, the M130 multipoint test was employed (50 fields per group, at 400x magnification). To the FGF-10, 50 images per group at 200× magnification were taken and evaluated at the QuPath software. All the $FGF\text{-}10^+$ cells were counted, and the total was divided by the section area, obtaining the number of $cells^+$ per mm^2. The stromal expression of FAP was also evaluated utilizing the M130 test.

2.4 | Immunofluorescence

This technique was employed to quantify total fibroblasts ($vim^+/\alpha\text{-}SMA^-$) and myofibroblasts ($vim^+/\alpha\text{-}SMA^+$) quantification. For this technique, a similar protocol to immunohistochemistry was used, differing in a few steps: after unspecific protein block, a mix with both primary antibodies (1:50 each) in BSA 1% in PBS was added to the samples and left overnight. To this technique, the following antibodies were used: vimentin (vim; Cell Signaling Technology, D21H3, 5741S, rabbit monoclonal) and smooth muscle α-actin (α-SMA; Santa Cruz Biotechnology Inc., sc-32251, H1111, mouse monoclonal). After, the samples were incubated with secondary antibodies Texas Red (TR; 1:50; sc-2780, 1:50, Santa Cruz Biotechnology Inc.; hosts: mouse and rabbit) or Fluorescein Isothiocyanate (FITC; 1:50; sc-2010, 1:50, Santa Cruz Biotechnology Inc.; hosts: mouse and rabbit) for 2 h. Then, slides were washed and mounted with 4′,6-diamidino-2-phenylindole (DAPI; Fluoroshield™ with DAPI, F6057, histology mounting medium, Merck), to nuclei distinguishment. Peroxidase blocking was not proceeded. Slides were analyzed using the Zeiss AX10 fluorescence microscope (Zeiss) and AxioVision Software (Zeiss). PBS (pH = 7.4) was used as the washing buffer. To quantify the stromal myofibroblasts and total fibroblasts, 50 fields per group, at 400× magnification were analyzed performing and adaptation of Weibel's technique where a total counting was employed and the cells divided by the total amount of 150 points/image).

2.5 | Transmission Electron Microscopy

For this technique, the samples fixed in glutaraldehyde 2.5% were post-fixed in osmium tetroxide 1%. Then, samples were dehydrated in a gradual progression of acetones (30% → 100%). Between fixation steps, the samples were washed with Millonig's phosphate buffer. Samples were pre-infiltrated with an araldite/acetone solution (1:1) overnight, followed by an infiltration in araldite (32°C) and an inclusion in araldite (48–72 h at 60°C). Semithin sections were performed for field analysis by Toluidine blue 1% staining. After field selection, ultrathin sections (50–70 nm) were performed in Leica Ultramicrotome (EM UC7), put on copper grids, and contrasted with 2% uranyl acetate (SPI-Chem Inc.) and 0.2% lead citrate (Merck). The image analysis was performed under the JEM-2100 Transmission Electron Microscope (Jeol) equipped with EDS (ThermoScientific) in the LabMic at the Federal University of Goiás (UFG).

2.6 | Statistical Analysis

Image-Pro Plus (v. 6.0) was used to cellular and growth factors quantification using a multifield counting technique. QuPath (v. 0.5.1; Bankhead et al. 2017) software was used to evaluate the FGF-10 expression. GraphPad Prism 8 (GraphPad Software, www.graphpad.com, v.8.0.1) and Microsoft Excel 2019 were used to graph assemble and to perform the following statistic tests: Shapiro–Wilk normality test; one-way ANOVA; Turkey's multi-comparison test. Data is expressed as relative frequency (%) ± standard deviation

and cells/mm^2 ± standard deviation. $\alpha = 5\%$ ($p \leq 0.05$) was adopted. In the blood vessels, the median and interquartile range (IQL) were also employed. In each technique employed, a total of 15 slides (5 slides per group) with 1 tissue sample were used to perform the quantification. A total of 10 photos of each sample were taken to perform both the multifield counting technique and QuPath quantification, totalizing 50 photos per group and 150 total.

3 | Results

3.1 | Fibroblastic Population and FGF-10 Expression

The analysis allowed to observe and quantify, due to vimentin and α-SMA double immunofluorescence, the fibroblasts (vim$^+$α-SMA$^-$) and myofibroblasts (vim$^+$α-SMA$^+$) population in the mammary gland reactive stroma (Figure 1A–F). The distribution of fibroblasts and myofibroblasts was found in the surrounding stroma of epithelial structures (Figure 1A–C), as well as into the lymph node (Figure 1D–E) of all groups. Total fibroblasts amount was similar in the control and BPA groups compared to vehicle group (Figure 1F). Although, the relative frequency (%) of total fibroblasts (vim$^+$α-SMA$^-$) was decreased in the BPA group (0.39% ± 0.16) compared to the control group (1.25% ± 0.68—$p = 0.0368$) (Figure 1F), myofibroblasts (vim$^+$α-SMA$^+$) were drastically increased in the BPA-exposed organ (1.38% ± 0.25) comparing to the control and vehicle groups (0.79% ± 0.23—$p = 0.033$; and 0.33% ± 0.34—$p = 0.0012$, respectively).

An increase in FAP$^+$ cells (Figure 2A) was also observed in the BPA group (6.52% ± 1.18) compared to the control (4.79% ± 0.88—$p = 0.045$) and vehicle groups (3.36% ± 0.67—$p = 0.0006$), observed in Figure 2B. The expression of FGF-10, a phenotypic fibroblastic inductor, was observed as cytoplasmic staining or a diffuse among extracellular matrix elements (Figure 2C). An increased FGF-10 stromal expression (Figure 2D) was observed in the BPA group (27.31% ± 2.04) compared to the control and vehicle groups (9.49% ± 2.34—$p < 0.0001$; and 1.4% ± 0.57—$p < 0.0001$, respectively).

3.2 | CD34+ Stromal Cells

By immunohistochemistry technique, CD34$^+$ cells were identified in stromal compartment (Figure 2E). These cells were observed among all experimental groups in stroma surrounding glandular epithelium and blood vessels. However, no statistical difference was observed when comparing all experimental groups (Figure 2F). The analysis was performed using relative frequency (%) by the multipoint technique, comprising all cellular extensions of these cells, such as telocytes and pericytes.

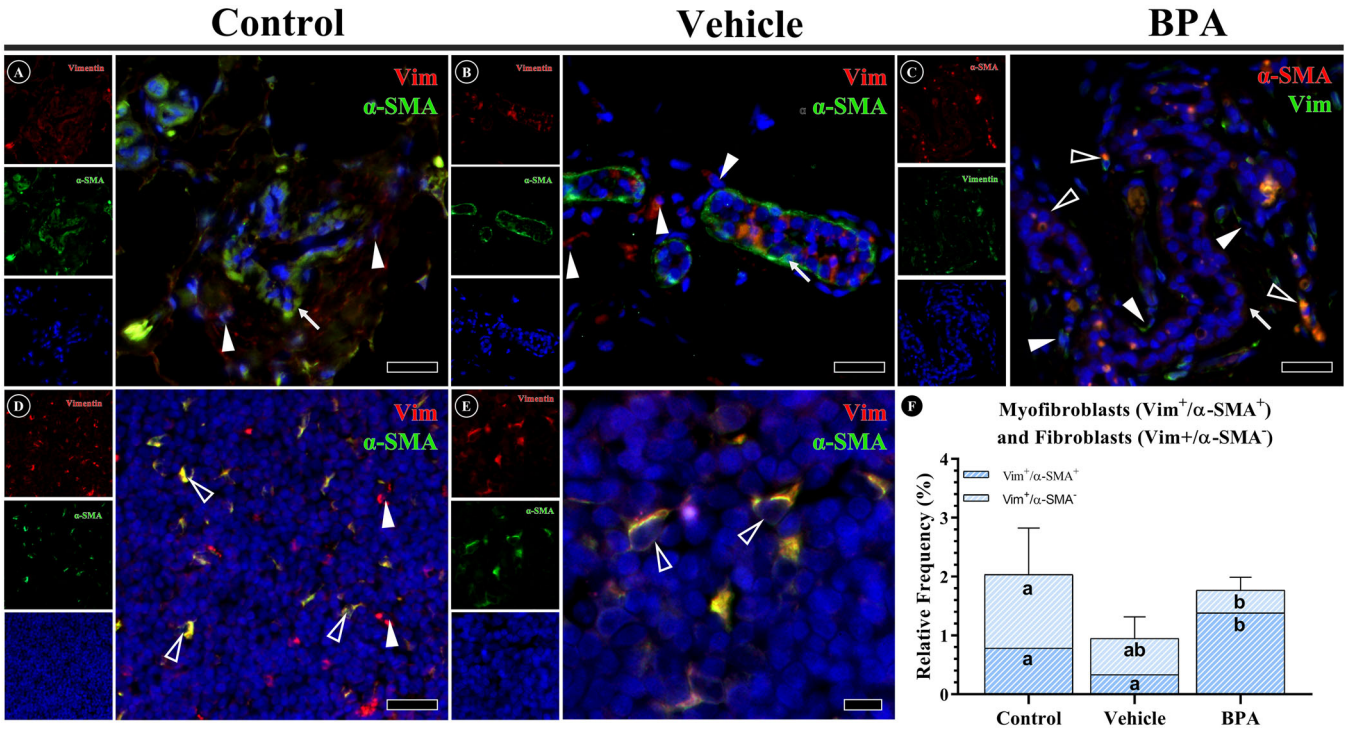

FIGURE 1 | Myofibroblasts and total fibroblasts of the mammary gland. (A–C) Glandular epithelium. Myofibroblasts (vim$^+$α-SMA$^+$) and fibroblasts (vim$^+$α-SMA$^-$) were identified in surrounding stroma among experimental groups. (D, E) MG lymph node was used as positive control for positive fibroblasts and myofibroblasts. (F) Data graph. Quantification of positive myofibroblasts and total fibroblast by immunofluorescence. Letters (a, b) indicate the significance and comparison among experimental groups. Myofibroblasts ANOVA p value: Control-BPA = $p = 0.033$; Vehicle-BPA = $p = 0.0012$. Total fibroblasts ANOVA p value: Control-BPA = $p = 0.0368$. Symbols: arrow: glandular epithelium (vim$^-$/α-SMA$^+$ for myoepithelial cells); black arrowhead: myofibroblasts (vim$^+$/α-SMA$^+$); white arrowhead: fibroblasts (vim$^+$/α-SMA$^-$). Scale bars: A–D = 20 μm; E: 10 μm.

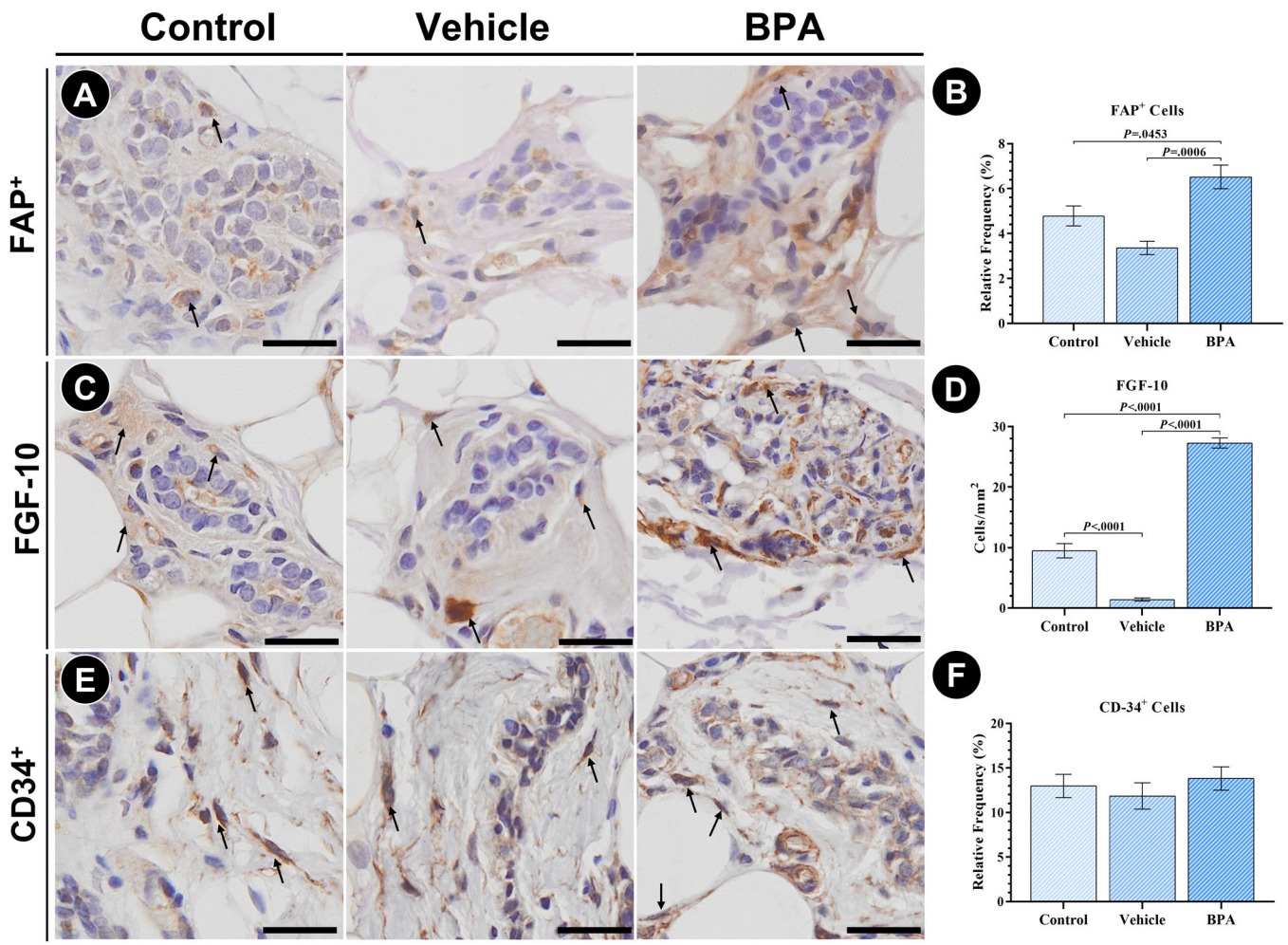

FIGURE 2 | Activated fibroblasts, CD34$^+$ stromal cells, and FGF-10 expression. (A, B) FAP$^+$ cells indicate activated fibroblast in the reactive stroma. (C, D) FGF-10 expression (cytoplasmic and diffuse staining). (E, F) CD34$^+$ stromal cells. Scale bars: 50 μm.

3.3 | Ultrastructural Identification of Stromal Cells

By transmission electron microscopy analysis, stromal cells were classified in surrounding stromal compartment. Previous analysis of semithin section provided a guide to identification of target cellular types in the stroma (Figure 3A–B). The control group (Figure 3A) presented normal morphology of fibroblastic population compared to the BPA, which demonstrated several features commonly associated with synthetic/activated phenotypes (Figure 3B). A strong-stained cytoplasmic with an evident nucleolus demonstrated the presence of myofibroblasts and activated fibroblasts in the stromal compartment of the BPA group (Figure 3B-insets). Telocytes-like cells were also observed in these sections, abundantly near to the epithelial compartment.

Under the transmission electron microscope, these features were clearly highlighted to precisely detect the cellular network (Figure 3C). The surrounding stroma of the BPA-exposed mammary glands presented myofibroblasts, telocytes, and active fibroblasts (Figure 3D–G). Myofibroblasts were characterized by the presence of electron dense structures in cytoplasm (Figure 3C). Also, a synthetic activity was detected due to the presence of new fibrillar content around these cells (Figure 3C). Telocytes were found near the epithelial compartment (Figure 3D–F) and among epithelial cells under endocrine disruption (Figure 3D) by the identification of its telopodes, podomers, and podoms among these cells. Although it was not possible to obtain a clear field with the nucleus, the characterization of telocytes was possible due to the clear podoms features, such as the presence of multiple mitochondria, multivesicular bodies, and endoplasmic reticulum (Figure 3E,F). Also, secretory activity was associated with telocytes since secretory vesicles and sites of elastin and collagen deposition were identified (Figure 3D). Activated fibroblasts were identified by the increased number of Golgi apparatus and rough endoplasmic reticulum, both with large cisternae and large nucleus (Figure 3G).

3.4 | Angiogenesis and VEGF

Blood vessels were quantified by the Gomori trichrome stain (Figure 4A). The BPA-exposed mammary glands presented an increase in the relative frequency of vascular supply (5.95% ± 0.64) compared to the control and vehicle groups (4.54% ± 0.59—$p = 0.0153$; and 3.53% ± 0.62—$p = 0.0002$, respectively) (Figure 4B). VEGF expression was observed in both stroma and epithelium of the organ (Figure 4C). A decrease in the BPA group, mainly in the epithelial expression (7.53% ± 1.94), was observed compared to the control group (10.6% ± 0.92—$p = 0.0367$). In contrast, was also

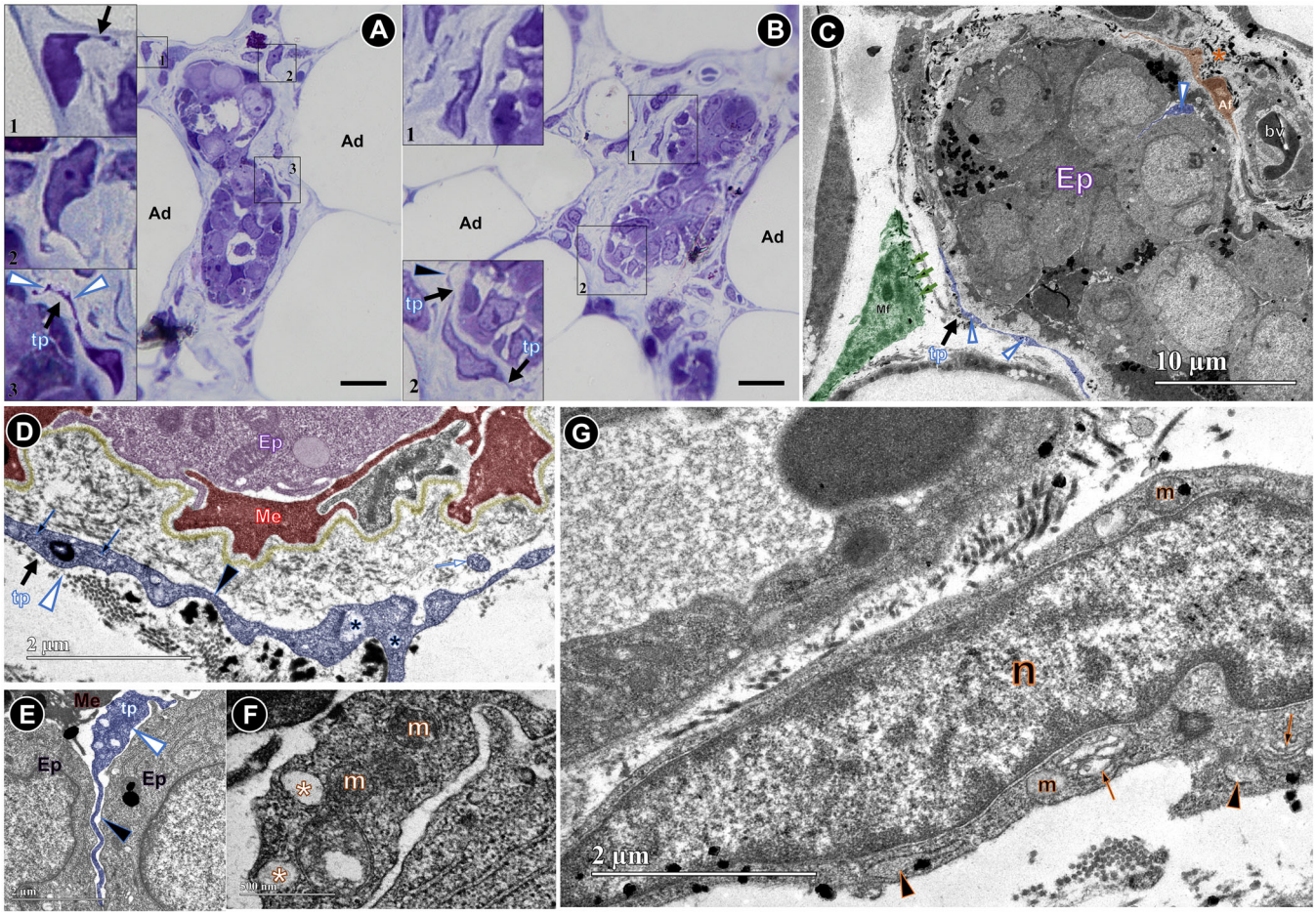

FIGURE 3 | Identification of reactive stromal cells. (A, B) Semi-thin sections of glandular epithelium and surrounding stroma of control and BPA groups, respectively. Insets indicate the morphology major cells identified. Telocyte-like cells were identified by telopodes (arrows) and podoms (white arrowheads). (C) Ultrastructure. Elements of reactive stroma surrounding glandular epithelium. Highlighted myofibroblast (green), active fibroblast (orange), and telocyte (blue) were demonstrated. For myofibroblast, a large nucleus with evident nucleoli was identified, and fibrillar components of extracellular matrix recently synthesized (green arrows). For active fibroblasts, the extracellular matrix (asterisk) was also identified. For telocyte, the projections of telopods (black arrow) and podoms (white arrowheads) were demonstrated. (D) Interface epithelium-stroma non-disrupted. MG glandular epithelium (purple) surrounded by myoepithelial cells (red), and in the surrounding stroma telopodes and podoms of telocytes. Basement membrane continuity was observed in these areas (yellow). (E, F) Telocyte invasion of epithelial compartment in disrupted areas. Multivesicular bodies (asterisks) and high mitochondrial content were found in the telopods. (G) Active fibroblast was described by large nucleus and synthetic apparatus. Large cisternae of Golgi apparatus (arrows) and rough endoplasmic reticulum (arrowheads), as well as mitochondrias, were present in the cytoplasm. Ep, epithelium; m, mitochondria; Me, myoepithelial cells; Mf, myofibroblast; Tp, telopodes.

observed an increased stromal expression in the BPA group ($8.2\% \pm 1.29$) compared to both control ($3.7\% \pm 1.05$—$p = 0.0105$) and vehicle groups ($3.6\% \pm 1.05$—$p = 0.0055$) (Figure 4D).

4 | Discussion

The present study aimed to analyze the modulation of main stromal cellular elements under a BPA pro-carcinogenic dosage exposure. Previous studies describe that aged gerbil females, when exposed to BPA during pregnancy and lactation, develop tumoral features in the epithelial compartment as the onset of mammary gland carcinogenesis (Leonel et al. 2021; Ruiz et al. Taboga, and Leonel 2021, 2023). The BPA group had a significant increase in myofibroblasts ($vim^+/\alpha\text{-}SMA^+$) and a decrease in fibroblasts ($vim^+/\alpha\text{-}SMA^-$), indicating a modulation in the total fibroblastic population in the mammary gland stroma. This increase suggests a transition from fibroblasts to myofibroblasts, accompanied by a rise in activated fibroblasts (FAP^+ cells), which alters the stromal microenvironment creating invasive conditions of the reactive stroma. The modulation of fibroblastic population arises as the main target of endocrine disruption, since other cells, such as $CD34^+$ cells, did not present significant differences among groups in surrounding gland stroma. These findings underscore the impact of BPA on cellular dynamics and have implications on the angiogenesis within the mammary gland stroma, as well as carcinogenic progression.

FAP^+ cells are found in normal tissue development, but they play important roles in pathological conditions. This protein is highly expressed in the stroma of most epithelial tumors and has an immunosuppressive character, being also expressed by stromal invasive cells (Hamson et al. 2014). However, the high

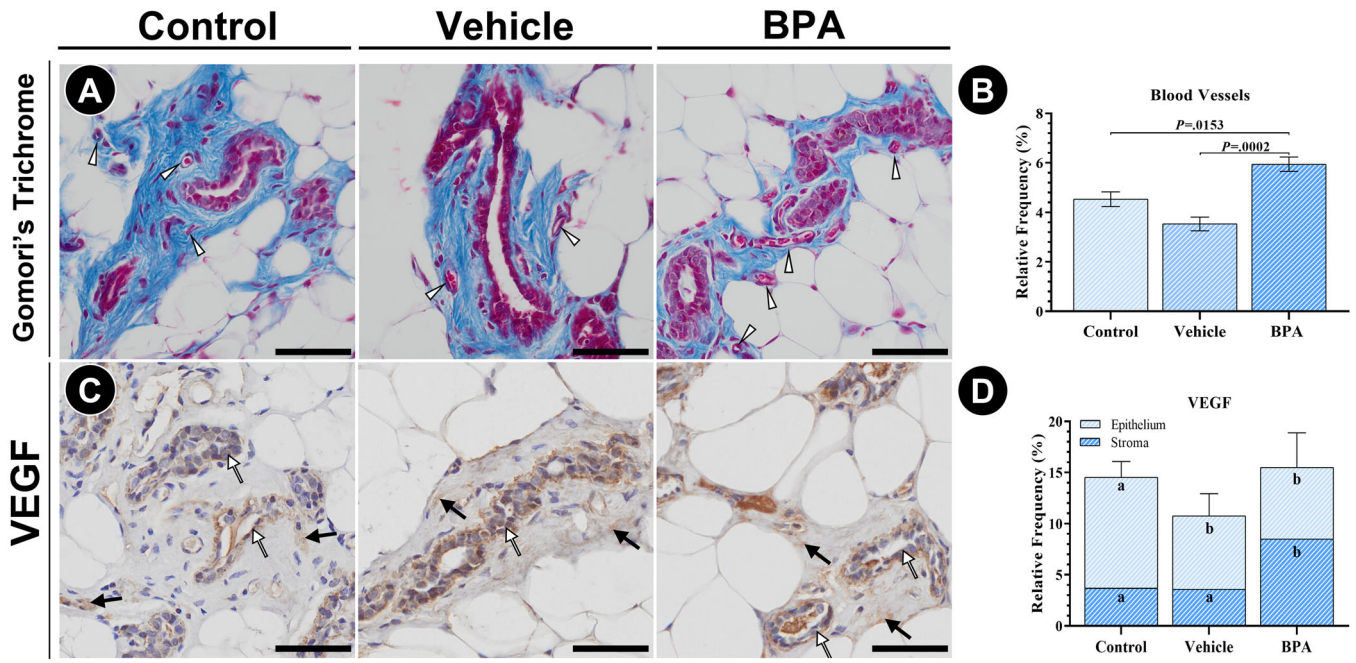

FIGURE 4 | Angiogenesis evaluation in the mammary gland. (A, B) Gomori's Trichrome for blood vessels. Arrowheads indicate small blood vessels and capillaries among collagenic stroma (blue stain). (C, D) VEGF expression by epithelial cells (white arrows) and diffuse in the stromal compartment (black arrows). Data graphs: Letters (a, b) indicate the significance and comparison among experimental groups. Epithelium ANOVA p-value: BPA-Control = $p = 0.0367$; Control-Vehicle = $p = 0.018$. Stroma ANOVA p-value: Control-BPA = $p = 0.0105$; Vehicle-BPA = $p = 0.0055$. Blood vessels mean/IQL range: Control: 4.6/1.1; Vehicle: 3.53/1.2; BPA: 5.871. Scale bars: 50 μm.

rates of FAP^+ cells are related to the occurrence of CAFs, tissue remodeling, and cancer progression (Tao et al. 2017). As observed in the present analyses, the BPA group showed high expression rates, suggesting an increase in fibroblasts activation and tumoral/cancer progression, as well as the worst prognosis for the BPA-exposed females. Despite that, it was observed a decrease in the typical fibroblast in the stroma and an increase in myofibroblasts. This downgrade of fibroblasts can be related, as mentioned previously, to an increase in fibroblasts rates followed by a transition to a morphologically different, more active, and invasive type of fibroblasts, the myofibroblasts (Michalik et al. 2018).

Myofibroblasts are stromal cells that present similar features of fibroblasts but with the ability of contraction, like smooth muscle cell, and playing an important role in tissue repair, being activated by stress conditions, and are commonly found in tissue damage regions (Pakshir et al. 2020). Nonetheless, when upregulated, it can also be related to tissue fibrosis (changing collagen microarchitecture), enhancing cancer progression and aggressiveness (Seo et al. 2020), leading to poor prognostics. Therefore, the elevated frequency of this cell type observed in the BPA group, compared to the control, suggests a damaged tissue with a possible change in extracellular matrix fibers, which can lead to tissue fibrosis, confirmed in a previous paper with the same experimental groups (Ruiz et al. 2021). This work demonstrated that the BPA-exposed gerbil females showed an increase in collagen and a decrease in elastic fibers in the mammary gland stroma surrounding the epithelium. Some myofibroblasts were also found in the gland lymph nodes in the BPA group. The presence of myofibroblasts in the lymph nodes can be a potentially major problem, as this cell type plays a major role in lymphoma tumoral microenvironment and, due to its pro-invasive action, associated to α-SMA expression, promotes metastasis to the lymph nodes (Catteau, Simon, and Noël 2014; Yeung et al. 2013). The uprise in these cell types occurred due to disruption in the tissue homeostasis, derived from the reactive stroma, leading to tissue rearrangement and tumoral progression (Brivio et al. 2017).

The high myofibroblastic increase observed can be related to FGF-10 high expression rates in the BPA-exposed groups, since this increased growth factor expression is related to epithelial-mesenchymal transition, which changes fibroblasts activity and alters the occurrence of epithelial and stromal breast cancer cell markers (Qazvini et al. 2019). The FGF-10 is a member of the FGF7 subfamily (composed of FGFs 3, 7, 10, and 22), who has a paracrine pathway and interacts with the fibroblast growth factor receptor 2 (Farooq et al. 2021). The FGF-10 expression is elevated in most human tumors and cancers (Rivetti et al. 2020). This growth factor regulates stromal tissue composition and plays an important role by regulating and targeting epithelial proliferation and branching mechanisms (Cui and Li 2013). Therefore, the high expression observed in the BPA group suggests an abnormal tissue development, as epithelial branching, and proliferation, that can corroborate to a tumoral microenvironment formation.

Another explanation for the myofibroblasts frequency observed in the BPA group is the increase of the transforming growth factor beta-1 (TGF-β_1) in the BPA-exposed females. There is observed an upregulation in TGF-β_1 expression after BPA exposition, as observed in a previous paper with these same experimental groups (Ruiz et al. 2022), being that higher

expression driving to fibroblasts transition. This growth factor is one of the inducers of the myofibroblast transition that leads to full expression of α-SMA by fibroblasts and, consequently, its contractile capability (Hinz et al. 2001). Thus, as the TGF-β_1 expression was elevated in the BPA group (as demonstrated in Ruiz et al. 2022), it can be assumed that myofibroblasts observed in the BPA-exposed group are mature and, therefore, more active. Also, as myofibroblasts show a capacity of cytokines and growth factors secretion, this uprise represents a significant driver in angiogenesis promotion due to VEGF secretion (Vong and Kalluri 2011).

$CD34^+$ stromal cells are interstitial cells that play important roles in extracellular matrix organization and are closely related to blood and lymphatic vessels (Díaz-Flores et al. 2021). These cells, along with pericytes, are important angiogenesis regulators, participating in blood vessels ramification (Díaz-Flores et al. 2022). An interesting finding in this study is the presence of telocyte cells in the mammary gland. Telocytes (TC) are interstitial cells, present in several organs, with a variable morphology and cytoplasm prolongments named telopodes (Pellegrini and Popescu 2011). These prolongments have a moniliform aspect with dilated zones called podoms (which presents important cellular functional unities) and thin segments called podomers (Cretoiu and Popescu 2014). TCs are linked to immunoregulatory capacity by releasing cytokines and modulating macrophages and B cells (Zhang and Tian 2023). They are also related to control tissue structure organization, microenvironment homeostasis, and especially, in females, a hormone-responsive character (TCs express estrogen and progesterone receptors in females' reproductive organs, as mammary glands) (Klein et al. 2022). Also, the presence of this cell type inside the epithelial compartment suggests both a tissue invasiveness due to the BPA exposition or an in-time relation of telocytes and the epithelial cells. As it is a newly identified cell type, further studies are needed for a better understanding of its function and role in both healthy and injured tissue. Although the $CD34^+$ cells did not show statistical difference between the groups, was observed a strong angiogenesis in the aged females after BPA exposition.

VEGF is a widely known growth factor related to endothelial cells migration and tissue wound healing (Farooq et al. 2021). However, its upregulation is related to invasive angiogenic blood vessels ramifications (Ucuzian et al. 2010). The VEGF expression was observed in all groups, both in epithelium and stroma, which can be related to this marker high expression rates in both health tissues and in tumors (Fukumura et al. 1998). Although it was observed a higher expression in the stroma and a decrease in the epithelial region of the BPA-exposed group, it is well known that the VEGF expression is severally related to malignant tumors than health tissue (Qiu et al. 2008). Also, VEGF induces TGF-β_1 angiogenesis capacity by stimulating endothelial cells survival, proliferation, and migration, as well as a necessary initial apoptotic effect (Ferrari et al. 2009). This angiogenic promotion of VEGF and TGF-β_1 is observed in the experimental groups since the BPA-exposed animals showed an increase in stromal blood vessels frequency. Therefore, the results obtained showed that BPA exposition can lead not only to a disturbance in the mammary gland stromal cell types and quantity but also promote changes in extracellular matrix composition and leads to a pro-angiogenic condition. These facts together enhance the capacity of a malignant tumoral phenotype formation.

5 | Conclusion

The results showed that exposure to BPA during periods of hormonal modulation, also known as windows of susceptibility, triggers the development of a phenotype known as reactive stroma during aging. The transition in fibroblasts morphology into a more active phenotype, related to an altered fiber production, was observed in the stromal compartment. The also observed increase in FGF-10 and stromal expression of VEGF is associated with the intensification of the cellular modification, as well as an angiogenesis intensification. Therefore, it was possible to observe that BPA exposition leads to a disruption in tissue homeostasis, with stromal cellular types change and increase in blood vessels formation, promoting the formation of a stromal environment conducive to tumorigenesis.

Author Contributions

Thalles Fernando Rocha Ruiz, **Ellen Cristina Rivas Leonel**, **Patricia Simone Leite Vilamaior**, and **Sebastião Roberto Taboga:** conceptualization. **Gervásio Evangelista Brito Filho**, **Thalles Fernando Rocha Ruiz**, **Lorena Gabriela de Souza**, **Luara Jesus Ferrato**, and **Fernanda Cristina Alcantara dos Santos:** methodology. **Sebastião Roberto Taboga**, **Thalles Fernando Rocha Ruiz**, **Ellen Cristina Rivas Leonel**, **Patricia Simone Leite Vilamaior**, and **Gervásio Evangelista Brito Filho:** investigation. **Sebastião Roberto Taboga**, **Thalles Fernando Rocha Ruiz**, **Fernanda Cristina Alcantara dos Santos**, **Patricia Simone Leite Vilamaior**, and **Ellen Cristina Rivas Leonel:** resources. **Thalles Fernando Rocha Ruiz**, **Gervásio Evangelista Brito Filho**, **Ellen Cristina Rivas Leonel**, and **Sebastião Roberto Taboga:** writing–original draft. **Thalles Fernando Rocha Ruiz**, **Gervásio Evangelista Brito Filho**, and **Sebastião Roberto Taboga:** writing–revised draft. **Sebastião Roberto Taboga:** supervision. **Sebastião Roberto Taboga** and **Thalles Fernando Rocha Ruiz:** funding acquisition.

Acknowledgments

The authors would like to thank the São Paulo State University – São José do Rio Preto campus (UNESP – IBILCE) for the structural support for this paper. Also, the Brazilian funding agencies FAPESP and CNPq. Fundação de Amparo à Pesquisa do Estado de São Paulo – Brazil (FAPESP), Grant Numbers: 2023/16098-1 (GEFB), 2022-00521-0 (TFRR), 2021/14140-5 (SRT); National Council for Scientific and Technological Development – Brazil (CNPq): Institutional Scientific Initiation Scholarship Program (PIBIC), Grant Number PROPe 04/2022; and Grant Number 302938/2020-6 (SRT).

Data Availability Statement

The data supporting this study are available on request from the corresponding author.

References

Abraham, A., and P. Chakraborty. 2019. "A Review on Sources and Health Impacts of Bisphenol A." *Reviews on Environmental Health* 35, no. 2: 201–210. https://doi.org/10.1515/reveh-2019-0034.

Bankhead, P., M. B. Loughrey, J. A. Fernández, et al. 2017. "Qupath: Open Source Software for Digital Pathology Image Analysis." *Scientific Reports* 7, no. 1: 16878. https://doi.org/10.1038/s41598-017-17204-5.

Barron, D. A., and D. R. Rowley. 2012. "The Reactive Stroma Microenvironment and Prostate Cancer Progression." *Endocrine-Related Cancer* 19: R187–R204. https://doi.org/10.1530/ERC-12-0085.

Biswas, S. K., S. Banerjee, G. W. Baker, C. Y. Kuo, and I. Chowdhury. 2022. "The Mammary Gland: Basic Structure and Molecular Signaling during Development." *International Journal of Molecular Sciences* 23, no. 7: 3883. https://doi.org/10.3390/IJMS23073883.

Brivio, S., M. Cadamuro, M. Strazzabosco, and L. Fabris. 2017. "Tumor Reactive Stroma in Cholangiocarcinoma: The Fuel Behind Cancer Aggressiveness." *World Journal of Hepatology* 9: 455–468. https://doi.org/10.4254/wjh.v9.i9.455.

Bujalance-Reyes, F., A. M. Molina-López, N. Ayala-Soldado, A. Lora-Benitez, R. Mora-Medina, and R. Moyano-Salvago. 2022. "Analysis of Indirect Biomarkers of Effect After Exposure to Low Doses of Bisphenol A in a Study of Successive Generations of Mice." *Animals: An Open Access Journal From MDPI* 12, no. 3: 300. https://doi.org/10.3390/ani12030300.

Bussard, K. M., L. Mutkus, K. Stumpf, C. Gomez-Manzano, and F. C. Marini. 2016. "Tumor-Associated Stromal Cells as Key Contributors to the Tumor Microenvironment." *Breast Cancer Research* 18, no. 1: 84. https://doi.org/10.1186/s13058-016-0740-2.

Catteau, X., P. Simon, and J. C. Noël. 2014. "Myofibroblastic Stromal Reaction and Lymph Node Status in Invasive Breast Carcinoma: Possible Role of the TGF-β1/TGF-βR1 Pathway." *BMC Cancer* 14, no. 1: 499. https://doi.org/10.1186/1471-2407-14-499/FIGURES/4.

Cretoiu, S. M., and L. M. Popescu. 2014. "Telocytes Revisited." *Biomolecular Concepts* 5: 353–369. https://doi.org/10.1515/bmc-2014-0029.

Cui, Y., and Q. Li. 2013. "Expression and Functions of Fibroblast Growth Factor 10 in the Mouse Mammary Gland." *International Journal of Molecular Sciences* 14, no. 2: 4094–4105. https://doi.org/10.3390/IJMS14024094.

Díaz-Flores, L., R. Gutiérrez, M. P. García, et al. 2021. "Cd34+ Stromal Cells/Telocytes in Normal and Pathological Skin." *International Journal of Molecular Sciences* 22, no. 14: 7342. https://doi.org/10.3390/IJMS22147342.

Díaz-Flores, L., R. Gutiérrez, M. P. García, et al. 2022. "Comparison of the Behavior of Perivascular Cells (Pericytes and CD34+ Stromal Cell/Telocytes) in Sprouting and Intussusceptive Angiogenesis." *International Journal of Molecular Sciences* 23, no. 16: 9010. https://doi.org/10.3390/IJMS23169010.

Farooq, M., A. W. Khan, M. S. Kim, and S. Choi. 2021. "The Role of Fibroblast Growth Factor (FGF) Signaling in Tissue Repair and Regeneration." *Cells* 10, no. 11: 3242. https://doi.org/10.3390/CELLS10113242.

Ferrari, G., B. D. Cook, V. Terushkin, G. Pintucci, and P. Mignatti. 2009. "Transforming Growth Factor-Beta 1 (TGF-β1) Induces Angiogenesis Through Vascular Endothelial Growth Factor (VEGF)-Mediated Apoptosis." *Journal of Cellular Physiology* 219, no. 2: 449–458. https://doi.org/10.1002/JCP.21706.

Fukumura, D., R. Xavier, T. Sugiura, et al. 1998. "Tumor Induction of VEGF Promoter Activity in Stromal Cells." *Cell* 94: 715–725.

Godfrey, M. 2009. "Extracellular Matrix." In *Asthma and COPD*, 265–274. Elsevier Ltd. https://doi.org/10.1016/B978-0-12-374001-4.00022-5.

Hamson, E. J., F. M. Keane, S. Tholen, O. Schilling, and M. D. Gorrell. 2014. "Understanding Fibroblast Activation Protein (FAP): Substrates, Activities, Expression and Targeting for Cancer Therapy." *Proteomics – Clinical Applications* 8, no. 5–6: 454–463. https://doi.org/10.1002/PRCA.201300095.

Hinz, B., G. Celetta, J. J. Tomasek, G. Gabbiani, and C. Chaponnier. 2001. "Alpha-Smooth Muscle Actin Expression Upregulates Fibroblast Contractile Activity." *Molecular Biology of the Cell* 12, no. 9: 2730–2741. https://doi.org/10.1091/MBC.12.9.2730/ASSET/IMAGES/LARGE/MK0911600008.JPEG.

Hu, F., W. Liang, L. Zhang, H. Wang, Z. Li, and Y. Zhou. 2022. "Hyperactivity of Basolateral Amygdala Mediates Behavioral Deficits in Mice Following Exposure to Bisphenol A and Its Analogue Alternative." *Chemosphere* 287: 132044. https://doi.org/10.1016/j.chemosphere.2021.132044.

Huang, Y. Q., C. K. C. Wong, J. S. Zheng, et al. 2012. "Bisphenol A (Bpa) in China: A Review of Sources, Environmental Levels, and Potential Human Health Impacts." *Environment International* 42, no. 1: 91–99. https://doi.org/10.1016/j.envint.2011.04.010.

Kalluri, R., and M. Zeisberg. 2006. "Fibroblasts in Cancer." *Nature Reviews Cancer* 6: 392–401. https://doi.org/10.1038/nrc1877.

Klein, M., M. Csöbönyeiová, Ľ. Danišovič, L. Lapides, and I. Varga. 2022. "Telocytes in the Female Reproductive System: Up-to-Date Knowledge, Challenges and Possible Clinical Applications." *Life* 12, no. 2: 267. https://doi.org/10.3390/LIFE12020267.

Lalonde, B., and C. Garron. 2020. "Spatial and Temporal Distribution of BPA in the Canadian Freshwater Environment." *Archives of Environmental Contamination and Toxicology* 78, no. 4: 568–578. https://doi.org/10.1007/s00244-020-00721-2.

Lambré, C., J. M. Barat Baviera, C. Bolognesi, et al. 2023. "Re-Evaluation of the Risks to Public Health Related to the Presence of Bisphenol A (BPA) in Foodstuffs." *EFSA Journal European Food Safety Authority* 21, no. 4: 06857. https://doi.org/10.2903/J.EFSA.2023.6857.

Leonel, E. C. R., S. G. P. Campos, C. M. B. Bedolo, et al. 2020. "Perinatal Exposure to Bisphenol A Impacts in the Mammary Gland Morphology of Adult Mongolian Gerbils." *Experimental and Molecular Pathology* 113: 104374. https://doi.org/10.1016/j.yexmp.2020.104374.

Leonel, E. C. R., T. F. R. Ruiz, C. M. Bedolo, S. G. P. Campos, and S. R. Taboga. 2021. "Inflammatory Repercussions in Female Steroid Responsive Glands After Perinatal Exposure to Bisphenol A and 17-β Estradiol." *Cell Biology International* 45, no. 11: 2264–2274. https://doi.org/10.1002/CBIN.11665.

Lind, P. M., and L. Lind. 2018. "Endocrine-Disrupting Chemicals and Risk of Diabetes: An Evidence-Based Review." *Diabetologia*: 1495–1502. https://doi.org/10.1007/s00125-018-4621-3.

Macias, H., and L. Hinck. 2012. "Mammary Gland Development." *Developmental Biology* 1: 533–557. https://doi.org/10.1002/wdev.35.

Manfo, F. P., R. Jubendradass, E. A. Nantia, P. F. Moundipa, and P. P. Mathur. 2014. "Adverse Effects of Bisphenol a on Male Reproductive Function." *Reviews of Environmental Contamination and Toxicology* 228: 57–82. https://doi.org/10.1007/978-3-319-01619-1_3.

Michalik, M., K. Wójcik-Pszczoła, M. Paw, et al. 2018. "Fibroblast-to-Myofibroblast Transition in Bronchial Asthma." *Cellular and Molecular Life Sciences* 75, no. 21: 3943–3961. https://doi.org/10.1007/S00018-018-2899-4.

Musumeci, G., P. Castrogiovanni, M. A. Szychlinska, et al. 2015. "Mammary Gland: From Embryogenesis to Adult Life." *Acta Histochemica* 117: 379–385. https://doi.org/10.1016/j.acthis.2015.02.013.

Nissen, N. I., M. Karsdal, and N. Willumsen. 2019. "Collagens and Cancer Associated Fibroblasts in the Reactive Stroma and its Relation to Cancer Biology." *Journal of Experimental and Clinical Cancer Research* 38: 115. https://doi.org/10.1186/s13046-019-1110-6.

Norris, M. L., and C. E. Adams. 1972. "Incidence of Cystic Ovaries and Reproductive Performance in the Mongolian Gerbil, Mer/Ones Ungu/Culatus." *Em Laboratory Animals* 6: 337–342.

Oehlmann, J., U. Schulte-Oehlmann, W. Kloas, et al. 2009. "A Critical Analysis of the Biological Impacts of Plasticizers on Wildlife." *Philosophical Transactions of the Royal Society, B: Biological Sciences* 364: 2047–2062. https://doi.org/10.1098/rstb.2008.0242.

Pakshir, P., N. Noskovicova, M. Lodyga, et al. 2020. "The Myofibroblast at a Glance." *Journal of Cell Science* 133, no. 13: jcs227900. https://doi.org/10.1242/JCS.227900/225072.

Pellegrini, M. S. F., and L. M. Popescu. 2011. "Telocytes." *Biomolecular Concepts* 2: 481–489. https://doi.org/10.1515/BMC.2011.039.

Qazvini, F. F., N. Samadi, M. Saffari, A. N. E. Razavi, and R. Shirkoohi. 2019. "Fibroblast Growth Factor-10 and Epithelialmesenchymal Transition in Colorectal Cancer." *EXCLI Journal* 18: 530–539. https://doi.org/10.17179/excli2018-1784.

Qiu, C. W., D. G. Lin, J. Q. Wang, C. Y. Li, and G. Z. Deng. 2008. "Expression and Significance of PTEN and VEGF in Canine Mammary Gland Tumours." *Veterinary Research Communications* 32, no. 6: 463–472. https://doi.org/10.1007/S11259-008-9049-7/TABLES/2.

Rivetti, S., C. Chen, C. Chen, and S. Bellusci. 2020. "Fgf10/Fgfr2b Signaling in Mammary Gland Development, Homeostasis, and Cancer." *Frontiers in Cell and Developmental Biology* 8: 415. https://doi.org/10.3389/fcell.2020.00415. www.frontiersin.org.

Ruiz, T., S. J. Colleta, D. Zuccari, P. Vilamaior, E. Leonel, and S. R. Taboga. 2021. "Hormone Receptor Expression in Aging Mammary Tissue and Carcinoma From a Rodent Model After Xenoestrogen Disruption." *Life Sciences* 285: 120010. https://doi.org/10.1016/j.lfs.2021.120010.

Ruiz, T. F. R., S. J. Colleta, E. C. R. Leonel, and S. R. Taboga. 2021. "Mammary Carcinoma in Aged Gerbil Mothers After Endocrine Disruption in Pregnancy and Lactation." *Endocrine-Related Cancer* 28, no. 11: 715–730. https://doi.org/10.1530/ERC-21-0198.

Ruiz, T. F. R., S. J. Colleta, D. D. dos Santos, et al. 2023. "Bisphenol A Disruption Promotes Mammary Tumor Microenvironment via Phenotypic Cell Polarization and Inflammatory Response." *Cell Biology International* 47, no. 6: 1136–1146. https://doi.org/10.1002/CBIN.12007.

Ruiz, T. F. R., E. C. R. Leonel, S. J. Colleta, C. M. Bedolo, S. G. Pegorin de Campos, and S. R. Taboga. 2022. "Gestational and Lactational Xenoestrogen Exposure Disrupts Morphology and Inflammatory Aspects in Mammary Gland of Gerbil Mothers During Involution." *Environmental Toxicology and Pharmacology* 89: 103785. https://doi.org/10.1016/j.etap.2021.103785.

Ruiz, T. F. R., S. R. Taboga, and E. C. R. Leonel. 2021. "Molecular Mechanisms of Mammary Gland Remodeling: A Review of the Homeostatic Versus Bisphenol A Disrupted Microenvironment." *Reproductive Toxicology* 105: 1–16. https://doi.org/10.1016/J.REPROTOX.2021.07.011.

San Martin, R., D. A. Barron, J. A. Tuxhorn, et al. 2014. "Recruitment of CD34+ Fibroblasts in Tumor-Associated Reactive Stroma." *American Journal of Pathology* 184, no. 6: 1860–1870. https://doi.org/10.1016/j.ajpath.2014.02.021.

Seo, B. R., X. Chen, L. Ling, et al. 2020. "Collagen Microarchitecture Mechanically Controls Myofibroblast Differentiation." *Proceedings of the National Academy of Sciences of the United States of America* 117, no. 21: 11387–11398. https://doi.org/10.1073/PNAS.1919394117/-/DCSUPPLEMENTAL.

Staples, C. A., P. B. Dorn, G. M. Klecka, S. T. O'Block, and L. R. Harris. 1998. "A Review of the Envorimental Fate, Effects, and Exposures of Bisphenol A." *Chemosphere* 36: 2149–2173.

Tao, L., G. Huang, H. Song, Y. Chen, and L. Chen. 2017. "Cancer Associated Fibroblasts: An Essential Role in the Tumor Microenvironment." *Oncology Letters* 14, no. 3: 2611–2620. https://doi.org/10.3892/ol.2017.6497.

Theocharis, A. D., S. S. Skandalis, C. Gialeli, and N. K. Karamanos. 2016. "Extracellular Matrix Structure." *Advanced Drug Delivery Reviews* 97: 4–27. https://doi.org/10.1016/j.addr.2015.11.001.

Tuxhorn, J. A., G. E. Ayala, D. R. Rowley, J. A. Tuxhorn, G. E. Ayala, and D. R. Rowley. 2001. "Reactive Stroma in Prostate Cancer Progression." *Journal of Urology* 166: 2472–2483.

Ucuzian, A. A., A. A. Gassman, A. T. East, and H. P. Greisler. 2010. "Molecular Mediators of Angiogenesis." *Journal of Burn Care & Research: Official Publication of the American Burn Association* 31, no. 1: 158–175. https://doi.org/10.1097/BCR.0B013E3181C7ED82.

Vandenberg, L. N. 2021. "Endocrine Disrupting Chemicals and the Mammary Gland." *Advances in Pharmacology* 92: 237–277. https://doi.org/10.1016/bs.apha.2021.04.005.

Vandenberg, L. N., R. Hauser, M. Marcus, N. Olea, and W. V. Welshons. 2007. "Human Exposure to Bisphenol A (BPA)." *Reproductive Toxicology* 24: 139–177. https://doi.org/10.1016/j.reprotox.2007.07.010.

Vong, S., and R. Kalluri. 2011. "The Role of Stromal Myofibroblast and Extracellular Matrix in Tumor Angiogenesis." *Genes & Cancer* 2, no. 12: 1139–1145. https://doi.org/10.1177/1947601911423940.

Weibel, E. R. 1963. "Principles and Methods for the Morphometric Study of the Lung and Other Organs." *Laboratory Investigation; A Journal of Technical Methods and Pathology* 12: 131–155. https://europepmc.org/article/med/13999512.

Xu, R., A. Boudreau, and M. J. Bissell. 2009. "Tissue Architecture and Function: Dynamic Reciprocity via Extra- and Intra-Cellular Matrices." *Cancer and Metastasis Reviews* 28, no. 1–2: 167–176. https://doi.org/10.1007/S10555-008-9178-Z.

Yeung, T. M., C. Buskens, L. M. Wang, N. J. Mortensen, and W. F. Bodmer. 2013. "Myofibroblast Activation in Colorectal Cancer Lymph Node Metastases." *British Journal of Cancer* 108, no. 10: 2106–2115. https://doi.org/10.1038/bjc.2013.209.

Zhang, Y., and H. Tian. 2023. "Telocytes and Inflammation: A Review." *Medicine* 102, no. 46: e35983. https://doi.org/10.1097/MD.0000000000035983.